Biomech Model Mechanobiol (2010) 9:629–640
DOI 10.1007/s10237-010-0202-1

ORIGINAL PAPER

Effects of curvature and cell–cell interaction on cell adhesion in microvessels

W. W. Yan · Y. Liu · B. M. Fu

Received: 27 August 2009 / Accepted: 23 February 2010 / Published online: 12 March 2010

Abstract It has been found that both circulating blood cells and tumor cells are more easily adherent to curved microvessels than straight ones. This motivated us to investigate numerically the effect of the curvature of the curved vessel on cell adhesion. In this study, the fluid dynamics was carried out by the lattice Boltzmann method (LBM), and the cell dynamics was governed by the Newton's law of translation and rotation. The adhesive dynamics model involved the effect of receptor-ligand bonds between circulating cells and endothelial cells (ECs). It is found that the curved vessel would increase the simultaneous bond number, and the probability of cell adhesion is increased consequently. The interaction between traveling cells would also affect the cell adhesion significantly. For two-cell case, the simultaneous bond number of the rear cell is increased significantly, and the curvature of microvessel further enhances the probability of cell adhesion.

Keywords Cell adhesion · Lattice Boltzmann method · Curved microvessel

1 Introduction

The cell adhesion under flow condition is a common phenomenon in microcirculation, e.g. adhesion of leukocytes and platelets for their immune and wound-healing functions, and adhesion of tumor cells to the microvessel wall during their metastasis. To date, significant advances have been made in cell adhesion. A major conceptual development is the recognition that cellular adhesions are often mediated via a surprisingly small number of receptor-ligand bonds (Zhu et al. 2000). It was found that, when the moving cells interact with a stationary surface in the flow chamber, the cell velocities are highly fluctuated and the cell motions experience "stop-and-go" jerky type (Kaplanski et al. 1993; Alon et al. 1995). Weiss (1992) found that successful cell arrest is dependent on the balance between adhesive and anti-adhesive forces, and the rate at which adhesive interactions are broken. Zhu (2000) and Zhu et al. (2000) presented a detailed review of the progress in the experimental methods that enable quantification of the relevant kinetic and mechanical parameters, the fundamental concepts that underlie the physics of the biological phenomena, and the mathematical models that relate functions to the intrinsic properties of the adhesion molecules.

It has been reported that the cell adhesion of leukocytes with the surface of ECs plays a crucial role in this inflammatory response (King and Hammer 2001a). Many in vitro studies of leukocytes adhesion were carried out using dilute cell suspension in flow chamber formed by two parallel plates (Munn et al. 1996). These experiments identified that the adhesion molecules on circulating leukocytes and the endothelium govern the leukocytes movement under hydrodynamic flow.

Haier and Nicolson (2001) reviewed the tumor cell adhesion under hydrodynamic conditions of fluid flow. They indicated that tumor cell adhesion to the microvasculature is a complex process involving various types of cell adhesion molecules. Experimental work at the nanoscale level to determine the lifetime, interaction distance, and strain responses of adhesion receptor-ligand bonds has been spurred by the advent of atomic force microscopy and biomolecular force

W. W. Yan · Y. Liu (✉)
Department of Mechanical Engineering,
The Hong Kong Polytechnic University, Kowloon, Hong Kong
e-mail: mmyliu@polyu.edu.hk

B. M. Fu
Department of Biomedical Engineering,
The City College of the City University of New York,
New York, NY, USA

probes (Marshall et al. 2003), although our current knowledge in this area is far from complete. Dong et al. (2005) studied human melanoma cell adhesion and migration under dynamic flow conditions using a modified Boyden chamber. Marshall et al. (2005) studied the force history dependence of receptor-ligand dissociation using atomic force microscopy that provided a new paradigm for understanding how force regulates receptor-ligand interactions. By measuring the change in thermal fluctuations of the atomic force microscope cantilever tip, Marshall et al. (2006) demonstrated the new measurement method of the molecular elasticity.

The extensive studies on biophysics of cell adhesion have also led to the development of a number of mathematical models. Hammer and Apte (1992) firstly proposed a mathematical model to simulate the interaction of a single rigid cell with a ligand-coated surface under flow. This model can simulate the effect of many parameters on adhesion, such as the number of receptors on microvillus tips, the density of ligands, the rates of reaction between receptors and ligands, the response of springs to strain, and the magnitude of the bulk hydrodynamic stresses. Since then, numerous simplifications, modifications, and refinements of adhesive dynamics models were proposed to simulate leukocyte adhesion (Dong et al. 1999), multiple leukocytes adhesion (King and Hammer 2001b), and leukocyte adhesion with deformable microvillus (Caputo and Hammer 2005).

In previous experimental and numerical work, most of the researchers paid attention to the cell adhesion in a straight chamber or a straight blood vessel, due to the simplicities to be carried out. However, in a recent experimental study (Liu et al. 2008), it was found that the curvature of blood vessels also had significant effect on cell adhesion. In this work, we investigate the cell adhesion in a curved microvessel by numerical method in two dimension. The cell was idealized as a disc circulating in the vessel and interacting with the surface of ECs by forming stochastic adhesive springs. The simulation dealt with both cell dynamics and fluid dynamics. The cell dynamics was carried out by the Newton's law with translation and rotation, and the fluid dynamics was implemented by the LBM. The so-called LBM has been a promising numerical tool to effectively model complex physics in computational fluid dynamics (CFD) (Chen and Doolen 1998), and it has simple formulations, efficient parallel computing, and can be easy to introduce complex boundary conditions.

2 Methods

2.1 Problem description

The schematic view of the 2-D curved microvessel is shown in Fig. 1. The vessel of diameter $D = 14\,\mu\text{m}$ starts with a straight segment and then a negatively bent segment of $\pi/3$ bending angle, with the inner curvature radius of $28\,\mu\text{m}$ and the outer radius of $42\,\mu\text{m}$, following with a positively curved segment with the inner and outer radii of 42 and $56\,\mu\text{m}$, respectively. The right half of the vessel is symmetric to the left half with the total vessel length of $L = 224\,\mu\text{m}$. Here, we used a cell of radius $r_C = 4.5\,\mu\text{m}$, a typical size of circulating leukocytes and tumor cells. The ratio of cell diameter to the vessel diameter is 0.64. The cell was initially placed in the straight part of vessel, and driven by a pressure difference Δp between the inlet at the left and the outlet at the right. The parameters and their values adopted are tabulated in Table 1.

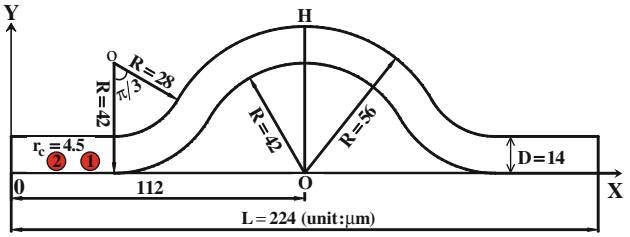

Fig. 1 Schematic view of a curved microvessel

Table 1 Simulation parameters and values

Parameter	Definition	Value
r_C	Cell radius	$4.5\,\mu\text{m}$
H_C	Critical length	40 nm
ε	Separation distance	
χ	Bond length	
λ	Equilibrium bond length	20 nm
ν	Plasma kinetic viscosity	$1.2 \times 10^{-6}\,\text{m}^2/\text{s}$
ρ_b	Plasma density	$1.03\,\text{g/m}^{-3}$
ρ_C	Cell density	$1.07\,\text{g/m}^{-3}$
A	Repulsive Hamaker constant	$5 \times 10^{-20}\,\text{J}$
T	Temperature	310 K
N_r	Receptor density	$47\,\mu\text{m}^2$
k_b	Boltzmann constant	$1.38 \times 10^{-23}\,\text{J/K}$
k_f^0	Intrinsic forward reaction rate	$10^{-2}\,\text{s}$
k_r^0	Intrinsic reverse reaction rate	$10^{-2}\,\mu\text{m}^2/\text{s}$
k_f	Forward reaction rate	
k_r	Reverse reaction rate	
P_f	Probability of bond formation	
P_r	Probability of bond breakage	
σ_{ts}	Transition state spring constant	$10^{-3}\,\text{N/m}$
σ	Spring constant	$2 \times 10^{-3}\,\text{N/m}$

2.2 Lattice Boltzmann model

The flow field is simulated by the lattice Boltzmann method. The Boltzmann equation describes the dynamics of non-

equilibrium processes and their relaxation to thermodynamic equilibrium. The lattice Boltzmann equation with the BGK collision operator (Bhatnagar et al. 1954) is

$$f_i(\vec{x}+\vec{e}_i\delta x, t+\delta t) - f_i\left(\vec{x}, t\right) = -\frac{1}{\tau}\left[f_i\left(\vec{x}, t\right) - f_i^{eq}\left(\vec{x}, t\right)\right], \quad i = 0, \ldots, N \tag{1}$$

where i indicates the direction of discrete velocity, $f_i\left(\vec{x}, t\right)$ is the distribution function for the particle with velocity $\vec{e}_i$ at position $\vec{x}$ and time t, δt is the time increment, δx is the length of lattice, $c = \delta x/\delta t$ is defined as the lattice speed, τ is the relaxation time, and $f_i^{eq}\left(\vec{x}, t\right)$ is the equilibrium distribution function. For D2Q9 (2 dimensions 9 velocities) model, the equilibrium distribution function can be chosen as

$$f_i^{eq}\left(\vec{x}, t\right) = \rho w_i\left(1 + \frac{3}{c^2}\left(\vec{e}_i \cdot \vec{u}\right) + \frac{9}{2c^4}\left(\vec{e}_i \cdot \vec{u}\right)^2 - \frac{3}{2c^2}u^2\right) \tag{2}$$

where w_i is the weight coefficients, and ρ and $\vec{u}$ are the macroscopic fluid density and fluid velocity, which can be calculated by particle distribution function via

$$\rho = \sum_{i=0}^{N=9} f_i\left(\vec{x}, t\right) = \sum_{i=0}^{N=9} f_i^{eq}\left(\vec{x}, t\right)$$
$$\rho\vec{u} = \sum_{i=0}^{N=9} \vec{e}_i f_i\left(\vec{x}, t\right) = \sum_{i=0}^{N=9} \vec{e}_i f_i^{eq}\left(\vec{x}, t\right). \tag{3}$$

2.3 Cell dynamics

The schematic view of a cell rolling on ECs wall with adhesive dynamic (receptor-ligand bonds) model in the microvessel is shown in Fig. 2. The cell was idealized as a disk, and the adhesion molecules on the tips of microvillus were modeled as receptors that distributed uniformly over the surface of the disc. The substrate is composed of ECs that have a high density of ligands. Once the distance between the receptor and the ligand is smaller than the critical length H_C, it has the chance to form receptor-ligand bonds.

The cell dynamics follows the Newton's law,

$$\frac{d\vec{u}_C}{dt} = \frac{\vec{F}_C}{m}, \quad I\frac{d\omega_C}{dt} = T_C \tag{4}$$

where $\vec{u}_C$ is the velocity of the center of mass of the cell, ω_C is the angular velocity, T_C is the torque, I is the inertia, m is the mass of cell, dt is the time step, and $\vec{F}_C$ is the total force acting on the cell. Here, $\vec{F}_C = \vec{F}_H + \vec{F}_S + \vec{F}_V$, where $\vec{F}_H$ is the hydrodynamic force, $\vec{F}_S$ is the total spring forces contributed by receptor-ligand bonds, and $\vec{F}_V$ is the repulsive van der Waals force. Here, $T_C = T_H + T_S$, where T_H and T_S are the torques induced by hydrodynamic and spring forces, respectively. At each time step, the position and rotational angle of cell were determined by

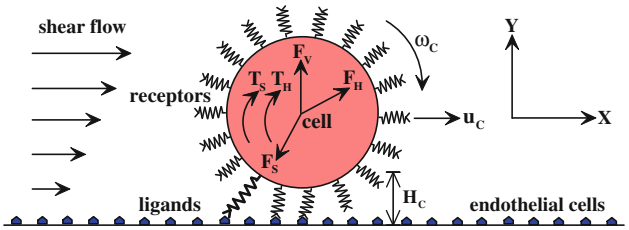

Fig. 2 Schematic view of the adhesive dynamics model

$$\frac{d\vec{x}_C}{dt} = \vec{u}_C, \quad \frac{d\theta_C}{dt} = \omega_C \tag{5}$$

For the purpose of stability, a "leap-frog" algorithm (Allen and Tildesley 1987) was adopted to update the position and velocity of cell with the increment of time

$$\vec{u}_C\left(t+\frac{1}{2}dt\right) = \vec{u}_C\left(t-\frac{1}{2}dt\right) + dt\cdot\frac{\vec{F}_C(t)}{m}$$
$$\vec{x}_C(t+dt) = \vec{x}_C(t) + dt\cdot\vec{u}_C\left(t-\frac{1}{2}dt\right) + dt^2\cdot\frac{\vec{F}_C(t)}{m}. \tag{6}$$

The angle and angular velocity of cell were updated in the same approach.

The hydrodynamic force was calculated by momentum exchange method (Ladd 1994). The repulsive van der Waals force (Bongrand and Bell 1984) was determined by

$$\vec{F}_V = \frac{A}{8\sqrt{2}}\sqrt{\frac{R_{\text{effective}}}{\varepsilon^5}} \tag{7}$$

where $R_{\text{effective}}$ is the effective radius, ε is the separation distance between the surfaces, and A is the repulsive Hamaker constant.

The adhesive force $\vec{F}_S$ was calculated based on the adhesion model of Hammer and Apte (1992), via the compression or expansion of adhesive springs (receptor-ligand bonds). The kinetic rate expressions between receptors and ligands, which relate the forward formation reaction rate k_f and reverse dissociation reaction rate k_r, extremely depend on the bond length χ. Dembo et al. (1988) demonstrated the reasonable, thermodynamically consistent rate expressions

Table 2 Validation results

	Normal force (pN)	Tangential force (pN)	Torque (pN × μm)	Pressure drop (Pa)	Cell velocity (μm/s)
Literature data	0.27−1.8[b,g]	45−450[a,d−g]	140−810[a,e,g]	1.2−4.5[d,e,g]	25−225[c,g]
Present result	0.32	65.23	207.9	1.5	163.65

[a] Goldman et al. (1967)
[b] Blackshear et al. (1971)
[c] Munn et al. (1996)
[d] Chapman and Cokelet (1997)
[e] Graver and Kute (1998)
[f] Dong et al. (1999)
[g] Migliorini et al. (2002)

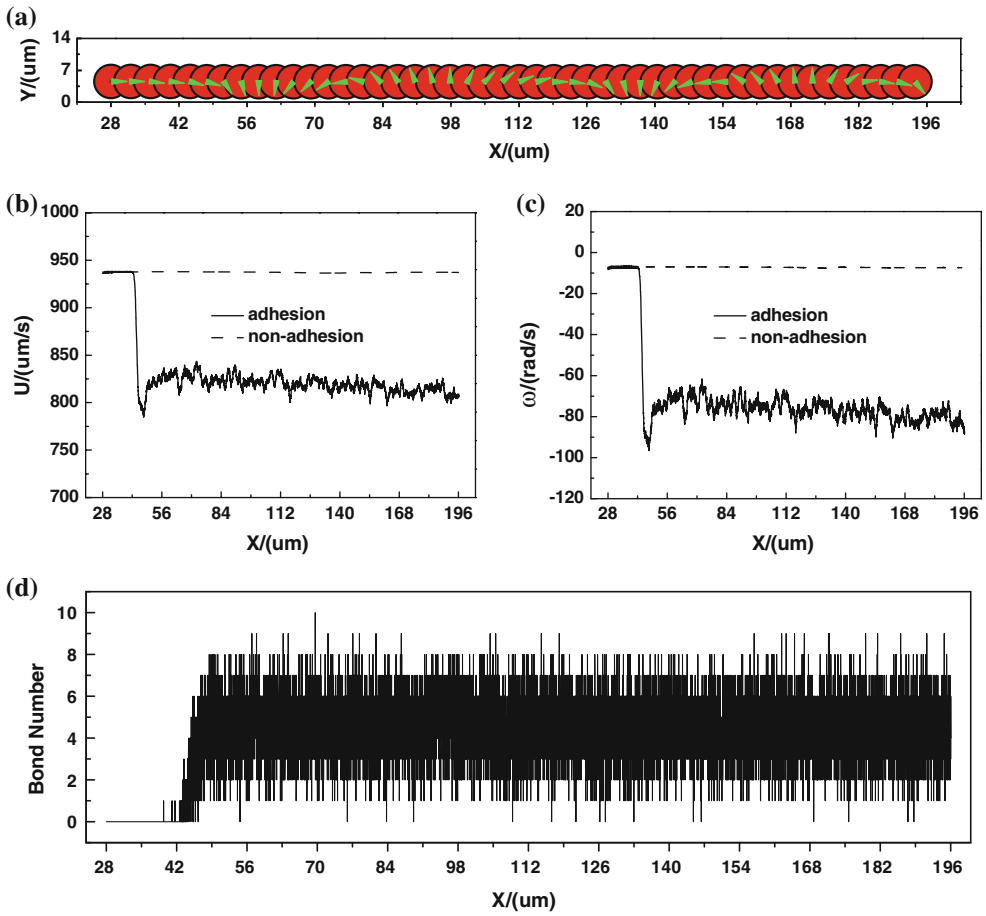

Fig. 3 The history of single cell with adhesion and non-adhesion in the straight micro vessel: **a** trajectory, **b** velocity, **c** angular velocity, and **d** bond number

relating these reaction rate constants to χ:

$$k_f = k_f^0 \exp\left(-\frac{\sigma_{ts}\,(\chi-\lambda)^2}{2k_bT}\right)$$
$$k_r = k_r^0 \exp\left(-\frac{(\sigma-\sigma_{ts})\,(\chi-\lambda)^2}{2k_bT}\right) \quad (8)$$

where k_b is the Boltzmann constant, T is the temperature, k_f^0 and k_r^0 are the reaction rate constants when the spring is at its equilibrium length, and σ_{ts} is a "transition state" spring constant.

The observed first-order rate of reaction for an adhesion molecule is $k_{on} = k_f \times N_r$, where N_r is the receptor density. The appropriate expressions for the probability of forming

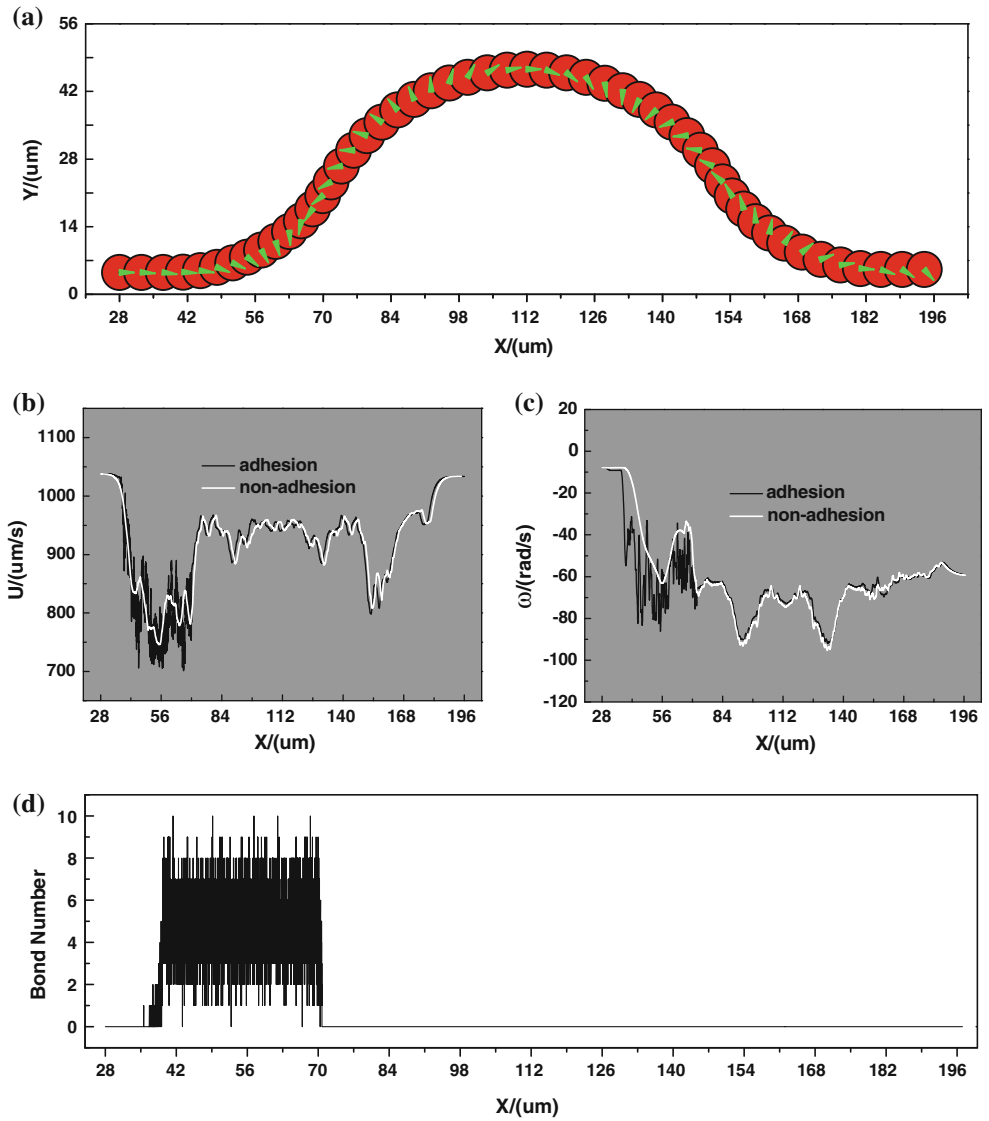

Fig. 4 The history of single cell with adhesion and non-adhesion in the curved micro vessel: **a** trajectory, **b** velocity, **c** angular velocity, and **d** bond number

and breaking tethers in a time step dt are (Chang and Hammer 1996):

$$P_f = 1 - \exp(-k_{on} dt)$$
$$P_r = 1 - \exp(-k_r dt) \tag{9}$$

where P_f is the probability of forming bonds, and P_r is the probability of breaking bonds in a time interval dt. The stochastic association and dissociation of inter-cell bonds were simulated using stochastic Monte Carlo technique by appropriate sampling of these probability expressions for each free and bond molecule during each time step.

Once a receptor-ligand bond is formed, assuming the spring constant is σ and equilibrium length is λ, the force of single spring applied by the bond on cell along the receptor-ligand direction is $\vec{F} = \sigma(\chi - \lambda)$. Therefore, the total adhesive force contributed by receptor-ligand bonds is the summation of all springs during each time step,

$$\vec{F}_S = \sum_{i=1}^{N} \sigma\,(\chi_i - \lambda) \tag{10}$$

where N is the number of bond in each time step.

3 Results and discussion

3.1 Single cell adhesion in a straight/curved microvessel

The validity of our numerical scheme is firstly examined by simulating the cell adhesion in a straight microvessel, and the validation problem is similar to that of Migliorini et al.

(2002), but the pressure drop is set as 1.5 Pa. The comparison of hydrodynamic normal force, tangential force, torque, and cell rolling velocity between our present results and other available data have been tabulated in Table 2. From the table, it is shown that our calculation is within the range of available results.

To evaluate the effect of vessel curvature on cell adhesion, the adhesion of a single cell in both straight and curved microvessels was studied first. To form receptor-ligand bonds easily, the cell was arranged near the wall of the microvessel at the entrance. Once the distance is within the critical length ($H_C = 0.04\,\mu$m), the cell movement would be influenced by the stochastic interactions between receptors and ligands. The pressure drop Δp between the inlet and outlet is set as 11.2 Pa (0.05 Pa/μm). Figure 3 shows the history of the single cell location and movement in a straight vessel with $\left(\vec{F}_S \neq 0\right)$ and without $\left(\vec{F}_S = 0\right)$ adhesion. Figure 3a shows the trajectory of the cell, which indicates a rolling effect of the cell due to cell adhesion. Figure 3b–c show the velocity and angular velocity of the cell, respectively. Compared to the velocity of non-adhesion case, the adhesion effect is obvious. At the entrance, the cell moves in the vessel with a constant velocity at about 940 μm/s, a normal velocity in this type of microvessels, indicating that the cell in this period is unattached. Then the velocity suddenly drops down to 800 μm/s, suggesting that the bond is being formed. After that point, the velocity experiences several fluctuations between 800 and 850 μm/s and keeps almost steadily fluctuating. The variation of angular velocity is very similar to that of the velocity. The angular velocity without adhesion is about 8.5 rad/s clockwise, and for the adhesion case, it fluctuates between 60 and 80 rad/s clockwise. Therefore, the adhesion enhances the cell rolling.

Figure 3d shows the history of how many bonds formed during the cell migration. The higher number of bonds means there is a larger opportunity for a cell to be caught. After off and on interactions between a circulating cell and the endothelium, the steady bonds are formed throughout the journey, which are represented by the black band in the figure. Most of the bond number fluctuates between 1 and 8 and very few reaches up to 10. These bonds result in the velocity and angular velocity oscillation as described in Fig. 3b–c.

For a single cell travels in a curved microvessel, the initial position of cell was set the same as that in the straight vessel. The pressure drop Δp between the inlet and outlet is set as 12.75 Pa (0.05 Pa/μm), i.e., the same pressure drop per unit length as that in a straight vessel. The history of cell motion with both adhesion and non-adhesion is illustrated in Fig. 4. From Fig. 4a, one can find that the cell translates and rotates around the curvature, and the total rotation angle is more than 4π, almost the same as that in a straight vessel. Figure 4b–c

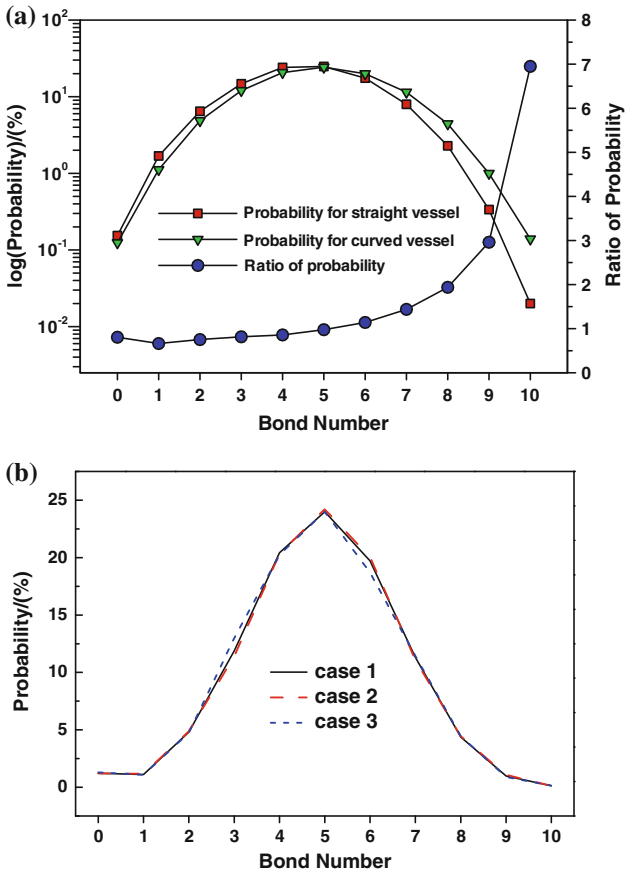

Fig. 5 **a** Comparison of bond formation probabilities and the ratio of the probabilities between the straight and curved microvessels. **b** Comparison of bond formation probabilities in the curved microvessel under same conditions

show that the effect of adhesion on velocity and angular velocity is not as significant as that in a straight vessel. The velocity is averaged over 20 μs using a moving average algorithm. Compared to the case of without adhesion, both the velocity and angular velocity profiles with adhesion generally follow that of no adhesion at the entrance of a curved vessel, but they are lower and fluctuating strongly due to the adhesion effect in the negative curvature vessel. Figure 4d shows the history of bond numbers. It is clearly shown that the bonds start to form at the entrance of the straight part of the curved vessel, and all the bonds are broken up at about $x = 70\,\mu$m where the flow has brought the cell off the microvessel wall. At the same location, the cell velocities of both with and without adhesions jump up as shown in Fig. 4b, indicating that the hydrodynamic force is dominant. During the binding period, the bond number fluctuates between 1 and 9, and a few reaches up to 10. Moreover, the cell adhesion only takes place at the entrance of the straight and negative curvature vessels. Once leaving the negative curvature vessel, the cell moves as a free cell, and there is no cell adhesion in the positive curvature vessel at all. Therefore, it can be

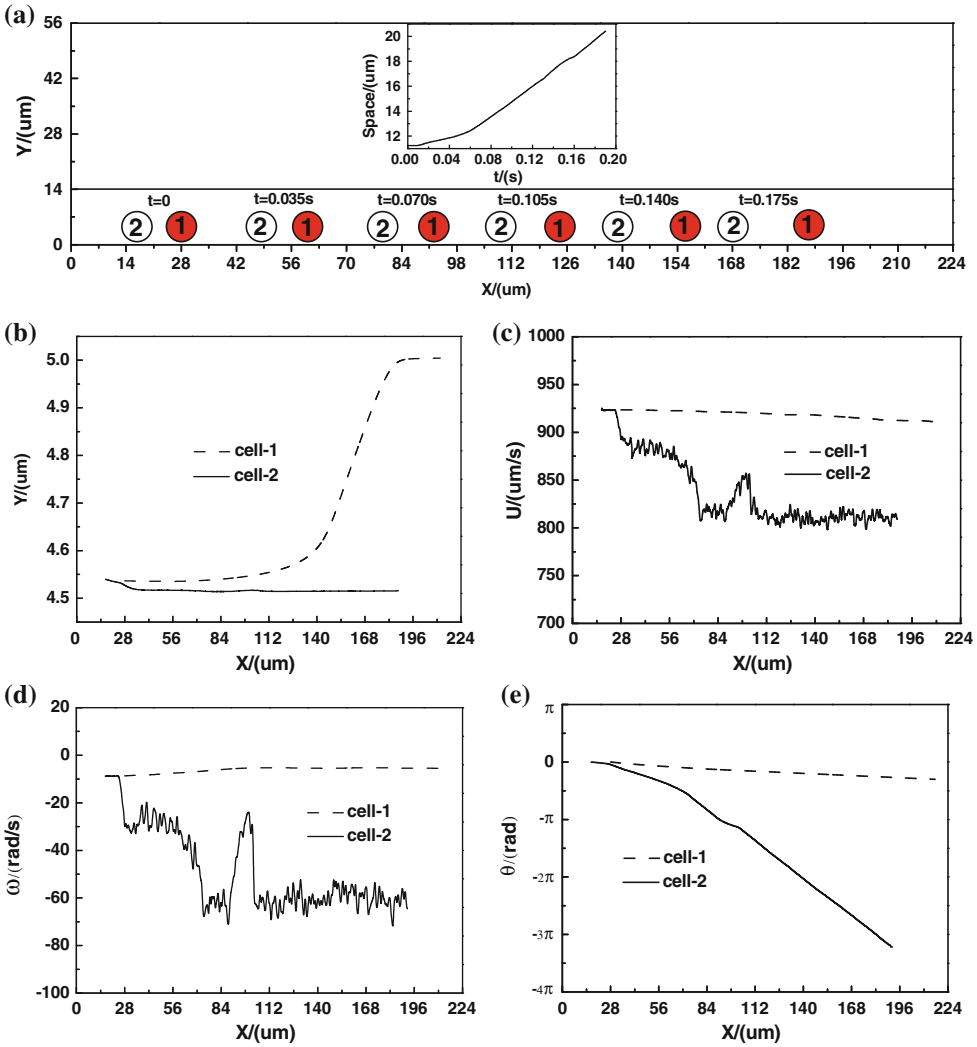

Fig. 6 The history of two cells adhesion in the straight micro vessel: **a** trajectory and spacing, **b** trajectory, **c** velocity, **d** angular velocity, **e** rotation angle, **f** bond number for cell-2, **g** relative flow vectors around cell-2 (frame is fixed on cell-2), **h** relative flow vectors around cell-1 (frame is fixed on cell-1), and **i** distribution of total perpendicular force along the vessel wall

concluded that the vessel curvature has significant influence on the cell adhesion.

To compare the probability of cell adhesion between the straight and curved vessels, the statistics of the bond number are calculated, and the probability of each bond number occurring and the ratio of these two probabilities are presented in Fig. 5a. It can be found that, for the smaller bond number, the adhesion probability in the straight vessel is larger than that in the curved vessel, and the turning point is at bond number being 5 with the probability of 25.5%. For the larger bond number, i.e. the bond number larger than 5, the probability in the curved vessel is obviously higher than that in the straight vessel, and the larger the bond number, the higher the probability in the curved vessel. It is understandable that the final cell adhesion depends on the bond numbers, the more the simultaneous bonds form, the higher probability the cell would adhere to the microvessel wall. Since we used a stochastic method to calculate the receptor-ligand binding, to evaluate the statistical significance, we calculated three cases for a curved microvessel under the same conditions, and found that the relative discrepancy is within 5%, as shown in Fig. 5b.

3.2 Adhesion and interaction of two cells in a straight/curved microvessel

The blood flow always involves multiple cells, and the interaction of the cells would affect the cell migration and adhesion. For simplicity, we firstly investigated two cells motion in a straight microvessel. Here, cell-1 was initially placed in

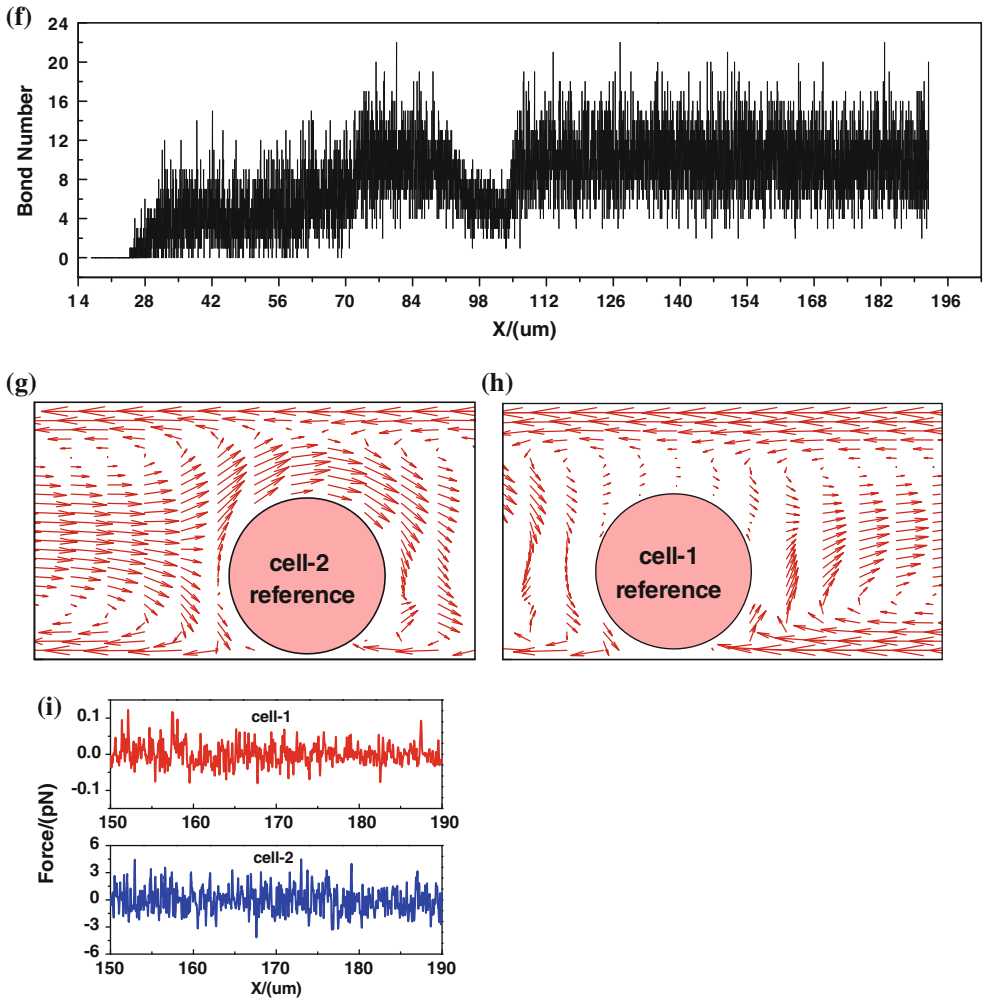

Fig. 6 continued

the same position as the single cell, and cell-2 was placed $0.5r_C$ behind cell-1. The pressure drop Δp is the same as that of a single cell. The history of the two cells' motion is illustrated in Fig. 6. The relative position of these two cells at different time is shown in Fig. 6a. The spacing between two cells becomes bigger and bigger, and the variation of the spacing with time is shown in the inset figure. The history of vertical spacing between the cell center and the wall is shown in Fig. 6b. Cell-1 moves away from the critical length, therefore it is difficult for cell-1 to form bonds during the journey. However, the spacing between cell-2 and the wall becomes smaller and smaller, and the adhesion is expected to occur. Figure 6c shows the history of velocity for both cells. Cell-1 moves in an almost constant velocity, but the velocity of cell-2 decreases and fluctuates due to the adhesion effect. Figure 6d–e clearly show the cell rotations and adhesion effects. The rotation speed of cell-1 is almost flat since there is no adhesion occurring. For cell-2, the angular velocity fluctuates apparently due to the adhesion effect. Generally, cell-1 would travel away from the wall under the interaction of cell-2, instead cell-2 would experience significant adhesive processes. Figure 6f shows the history of bond number of cell-2. Due to the interaction with cell-1, the bond number of cell-2 is obviously larger than that of a single cell, and the maximum bond number can reach up to 22, more than twice the bond number in the single cell case. Unlike that in the single cell adhesion, the bond number of cell-2 experiences an unstable variation, and then reaches a steady bond number state. To further elaborate on this phenomenon, the relative flow vectors around each cell are plotted in Fig. 6g–h. The cells not only translate but also rotate, and the relative vectors are actually relative to the translation only. Around cell-2, the fluid moves faster than the cell and the flow vectors are close and clockwise around the cell. In contrast, around cell-1, the relative flow vectors are very small, indicating the speed of cell-1 is almost the same as that of surrounding fluid. Figure 6i plots the total perpendicular force of each cell along the vessel where the negative sign indicates toward the wall

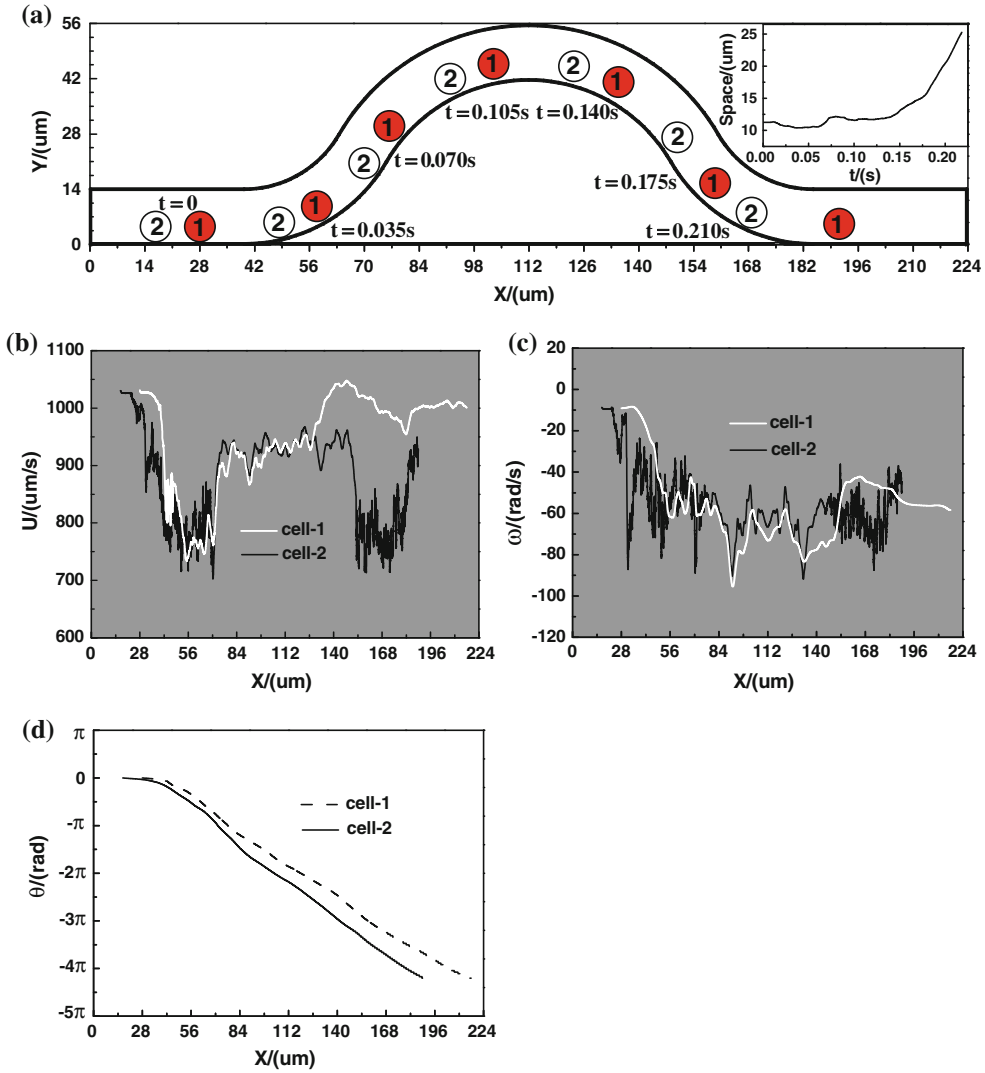

Fig. 7 The history of two cells adhesion in the curved micro vessel: **a** trajectory and spacing, **b** velocity, **c** angular velocity, **d** rotation angle, **e** bond number for cell-1, **f** bond number for cell-2, **g** relative flow vectors around cell-1 (frame is fixed on cell-1), **h** relative flow vectors around cell-2 (frame is fixed on cell-2), and **i** distribution of total perpendicular force along the vessel wall

(wallward). The wallward force on cell-2 is much larger than that on cell-1, which pushes cell-2 to the wall, resulting in much more receptor-ligand binding than cell-1.

Figure 7 shows the history of two-cell adhesion in a curved vessel where the initial position and pressure drop are the same as those of the straight vessel. Similar to the single cell case, the cell speed is averaged over 20 μs. Figure 7a shows the relative position of the two cells at different times, the spacing between the two cells is almost constant in the bend and becomes larger out of the bend. The speed of both cells experiences significant fluctuations due to the adhesion and curvature effect, as indicated in Fig. 7b. The speed of cell-1 firstly drops from 1,030 to 800 μm/s due to the adhesion, then the cell-1 moves like a free cell, and its velocity increases and experiences several fluctuations. However, the speed of cell-2 experiences two valleys, the distribution is almost symmetric and follows the curved geometry, indicating the adhesion occurs at both the entrance and exit of the curved vessel. Figure 7c shows a strong oscillation of the angular velocity due to the coupled effect of adhesion and cell–cell interaction. It is interesting to note that the rotating angle of the two cells is almost the same as shown in Fig. 7d, even the adhesion status and the flow field of each cell are quite different. The number of bonds in cell-1 and cell-2 are illustrated in Fig. 7e, f, respectively. Compared to the single cell adhesion in the curved vessel, the bond number of cell-1 is much smaller, and the adhesive length is much shorter. There is nearly no adhesion for cell-1. However, the bond number of cell-2 increases significantly, the highest bond number reaches 23, and the adhesion occurs at both the entrance and exit of the curved

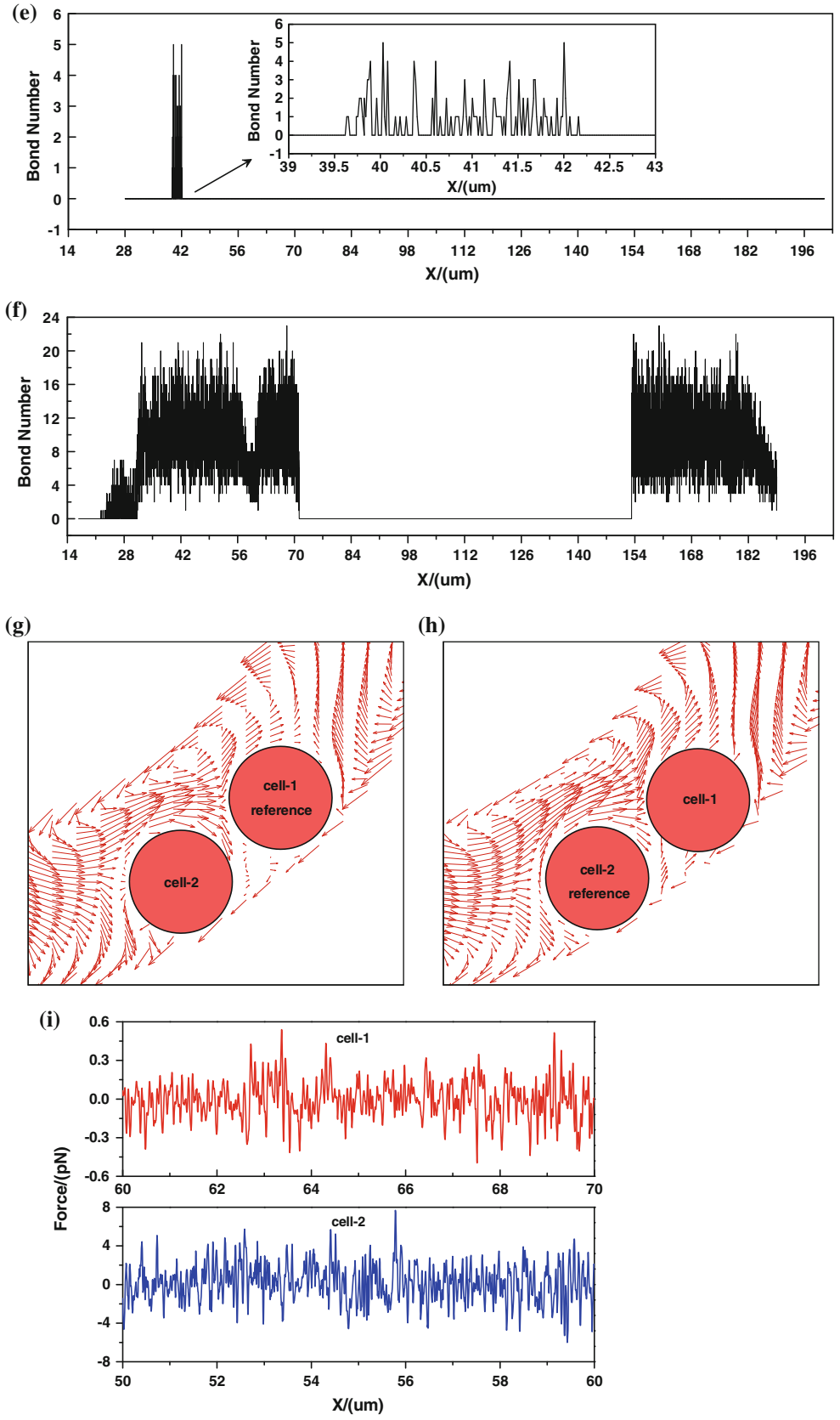

Fig. 7 continued

vessel. The number of the bonds at cell-2 changes dramatically during the whole process. Firstly, the cell rolls as a free cell, since there is no bond formed from the initial position to $x = 22\,\mu$m. Then the bond number increases from 1 to 7 in the straight part of the vessel. Once entering the curved part of the vessel, the bond number augments quickly. Then there is a sharp drop in the bond number at $x = 59\,\mu$m. A possible explanation for this is that, with the increment of bonds formed, the distance between the moving cell and ECs at the wall is so close that the repulsive van der Waals force is big enough to expel the cell. When the cell moves into the positive curvature vessel, there is no bond found in that domain at all. In contrast, like the situation in the negative curvature vessel near the inlet, there are many bonds formed with the same peak and similar average value in the negative curvature vessel near the outlet. To further investigate the effect of curvature on receptor-ligand binding, the relative flow vectors around each cell are plotted in Fig. 7g, h, respectively. Figure 7i shows the distribution of total perpendicular force along the vessel wall. Similar to the straight vessel, the perpendicular force also exhibits the oscillatory pattern; the oscillating amplitude of cell-2 is much larger than that of cell-1. Specifically, the magnitude of the wallward force on cell-2 in the curved vessel is about 1.6 times of that in the straight vessel. This explains why cell-2 generates more receptor-ligand bonds in the curved vessel than that in the straight one. From above analysis, we can conclude that the cell adhesion is strongly dependent on local geometry of the vessel and the interaction with other cells.

Figure 8 shows the statistical comparison of bond numbers for cell-2 between the straight and curved vessels. Similar to the single cell case, at lower bond numbers, the straight vessel has higher probability to form the bonds. The turning point is at the bond number of 8. When the bond number is larger than 8, the curved vessel has more chances to form bonds between cell-2 and the ECs at the vessel wall. At higher bond number, e.g. bond number of 21 or more, the bond forming probability of the curved vessel can be five times that of the straight vessel. As discussed earlier, the final cell adhesion is actually dependent on the simultaneous bond forming. The higher the bond number, the more likely cell adhesion occurs. Therefore, the cell, particularly under the interaction of other cells, has higher probability to adhere to the ECs in the curved vessel than in the straight vessel.

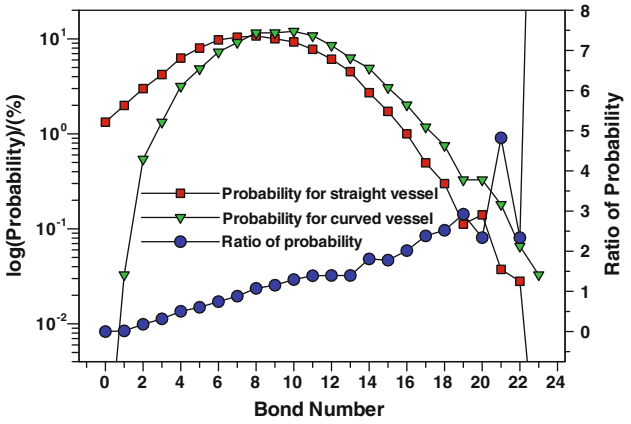

Fig. 8 Comparison of bond formation probabilities and the ratio of the probabilities between the straight and curved microvessels

4 Conclusion

The effects of the curvature and the cell–cell interaction on cell adhesion in the microvessels has been numerically studied using the LBM method, and the cell adhesive dynamics is modeled by adhesive spring (receptor-ligand bond) model. Both the single cell and double cells in either the straight or the curved vessel have been investigated. The simulation results lead to the following conclusions:

(1) The local geometry or the curvature has significant influence on bond formation between traveling cells and the ECs at the vessel wall. Usually, the simultaneous bond number would increase in a curved vessel, consequently the probability of cell adhesion is increased as well.
(2) The interaction between the traveling cells is significant, and the cell-2 (rear) would experience higher wallward force, which would enhance the receptor-ligand binding, consequently, this interaction would increase the cell adhesion probabilities.
(3) From a physiological point of view, most of the microvessels are either curved or bifurcated and there are always multiple cells traveling in the same microvessel. The above conclusions indicate that the study of the single cell adhesion in a straight vessel may underestimate the capability of cell adhesion in the microvessels under real physiological and pathological conditions.

Acknowledgments Supports by the Research Grants Council of the Government of the HKSAR under Grant No. PolyU 5238/08E and the Hong Kong Polytechnic University through a scholarship to WWY are gratefully acknowledged. The support from the US National Science Foundation under grant No. CBET 0754158 is also acknowledged. We thank Dr. Hua-bing Li for his helpful discussion about the lattice Boltzmann simulation.

References

Allen MP, Tildesley DJ (1987) Computer simulation of liquid. Clarendonn, Oxford

Alon R, Hammer DA, Springer TA (1995) Lifetime of the P-selectin carbohydrate bond and its response to tensile force in hydrodynamic flow. Nature 374:539–542

Bhatnagar PL, Gross EP, Krook M (1954) A model for collision processes in gases. I. Small amplitude processes in charged and neutral one-component systems. Phys Rev 94:511–525

Blackshear PL, Forstrom RJ, Dorman FD, Voss GO (1971) Effect of flow on cells near walls. Fed Proc 30:1600–1611

Bongrand P, Bell GI (1984) Cell-cell adhesion: parameters and possible mechanisms. In: Perelson A, DeLisi C, Wiegel FW (eds) Cell surface dynamics: concepts and models. Marcel Dekker, New York

Caputo KE, Hammer DA (2005) Effect of microvillus deformability on leukocyte adhesion explored using adhesive dynamics simulations. Biophys J 89:187–200

Chang KC, Hammer DA (1996) Influence of direction and type of applied force on the detachment of macromolecularly-bound particles from surfaces. Langmuir 12:2271–2282

Chapman GB, Cokelet GR (1997) Model studies of leukocyte endothelium-blood interaction. Biorheology 34:37–56

Chen S, Doolen GD (1998) Lattice Boltzmann method for fluid flows. Annu Rev Fluid Mech 30:329–364

Dembo M, Torney DC, Saxman K, Hammer DA (1988) The reaction-limited kinetics of membrane-to-surface adhesion and detachment. Proc R Soc Lond B Biol Sci 234:55–83

Dong C, Cao J, Struble EJ, Lipowksy HH (1999) Mechanics of leukocyte deformation and adhesion to endothelium in shear flow. Ann Biomed Eng 27:298–312

Dong C, Slattery M, Liang SL (2005) Micromechanics of tumor cell adhesion and migration under dynamic flow conditions. Front Biosci 10:379–384

Goldman AJ, Cox RG, Brenner H (1967) Slow viscous motion of a sphere parallel to a plane wall-II Couette flow. Chem Eng Sci 22:653–660

Graver DP, Kute SM (1998) A theoretical study of the influence of fluid stresses on a cell adhering to a microchannel wall. Biophys J 75:721–733

Haier J, Nicolson GL (2001) Tumor cell adhesion under hydrodynamic conditions of fluid flow. APMIS 109:241–262

Hammer DA, Apte SM (1992) Simulation of cell rolling and adhesion on surfaces in shear flow: general results and analysis of selectin-mediated neutrophil adhesion. Biophys J 63:35–57

Kaplanski G, Farnarier C, Tissot O, Pierres A, Benoliel AM, Alessi MC, Kaplanski S, Bongrand P (1993) Granulocyte-endothelium initial adhesion. Analysis of transient binding events mediated by E-selectin in a laminar shear flow. Biophys J 64:1922–1933

King MR, Hammer DA (2001a) Multiparticle adhesive dynamics: hydrodynamic recruitment of rolling leukocytes. PNAS 98:14919–14924

King MR, Hammer DA (2001b) Multiparticle adhesive dynamics. Interactions between Stably Rolling Cells. Biophys J 81:799–813

Ladd ACJ (1994) Numerical simulation of particulate suspensions via a discretized Boltzmann equation: Part 1. Theoretical foundation. J Fluid Mech 271:285–309

Liu Q, Mirc D, Fu BM (2008) Mechanical mechanisms of thrombosis in intact bent microvessels of rat mesentery. J Biomech 41:2726–2734

Marshall BT, Long M, Piper JW, Yago T, McEver RP, Zhu C (2003) Direct observation of catch bonds involving cell-adhesion molecules. Nature 423:180–193

Marshall BT, Sarangapani KK, Lou JZ, McEver RP, Zhu C (2005) Force history dependence of receptor-ligand dissociation. Biophys J 88:1458–1466

Marshall BT, Sarangapani KK, Wu JH, Lawrence MB, McEver RP, Zhu C (2006) Measuring molecular elasticity by atomic force microscope cantilever fluctuations. Biophys J 90:681–692

Migliorini C, Qian YH, Chen HD, Brown EB, Jain RK, Munn LL (2002) Red blood cells augment leukocyte rolling in a virtual blood vessel. Biophys J 83:1834–1841

Munn LL, Melder RJ, Jain RK (1996) Role of erythrocytes in leukocyte-endothelial interactions: mathematical model and experimental validation. Biophys J 71:466–478

Weiss L (1992) Biomechanical interactions of cancer-cells with the microvasculature during hematogenous metastasis. Cancer Metastasis Rev 11:227–235

Zhu C (2000) Kinetics and mechanics of cell adhesion. J Biomech 33:23–33

Zhu C, Bao G, Wang N (2000) Cell mechanics: mechanical response, cell adhesion, and molecular deformation, Annu. Rev Biomed Eng 2:189–226